CAN ULTRASOUND IN COMBINATION WITH VIRTUAL TOUCH IMAGING QUANTIFICATION PREDICT THE DIGNITY OF A PAROTID TUMOR?

MONIKA JERING,* JOHANNES ZENK,* RUBENS THÖLKEN,* HOLGER RÜGER,* and GEORGIOS PSYCHOGIOS*,†

* Department of Otolaryngology, Head and Neck Surgery, University Hospital Augsburg, Augsburg, Germany; and † Department of Otolaryngology, Head and Neck Surgery, University Hospital of Ioannina, Ioannina, Greece

INTRODUCTION

Ultrasonography constitutes an important, non-invasive tool in the pre-operative evaluation of parotid gland lesions and provides the surgeon with useful information regarding configuration, size and location of the tumor (Klintworth et al. 2012; Bozzato 2015; Zengel et al. 2018; Psychogios et al. 2019). A malignant tumor of the parotid gland can be identified in 90.0% of cases by a skilled sonographer, thus obviating the need for additional pre-operative testing and minimizing the danger of re-operation because of unexpected malignancy. Sonographic findings of echogenicity, perfusion, tissue stiffness and tumor margins can help distinguish malignant from benign tumors (Mansour et al. 2017).

More recently, shear wave elastography has been developed to help differentiate malignant from benign tumors based on a quantitative assessment of tissue stiffness. In an early stage of malignancy, tissue stiffness increases because of an increase in vascularity, infiltration with cancer and inflammatory cells, deposition of extracellular matrix and expansion of the tumor-associated cellular stroma (Matsuzuka et al. 2015). Through these pathologic mechanisms, malignancies may alter tissue elasticity. Several small studies have reported that within the parotid gland, tissue stiffness, as quantified by shear wave elastography, is higher in malignant lesions compared with healthy tissue or benign tumors (Matsuzuka et al. 2015; Zengel et al. 2018). Shear wave elastography can define the mechanical properties of various tissues by measuring the propagation speed of shear waves through tissue. With Virtual Touch imaging quantification elastography (VTIQ) (Acuson S2000, Siemens Medical Solution, Erlangen, Germany), tissue is subjected to a series of acoustic radiation force impulses (Azizi et al. 2016); the resultant tissue displacement creates a shear wave propagation front. Propagation of shear waves depends on tissue stiffness, with stiffer tissue allowing for faster propagation of shear waves (Cheng et al. 2016). Propagation of shear waves is measured by the emitting probe within predefined regions of interest and is then converted into a color-coded image, superimposed on the B-mode ultrasound images. The image displayed is formed by a pulse sequence, and tracking vectors are calculated. Within the color-coded

Address correspondence to: Monika Jering, Department of Otolaryngology, Head and Neck Surgery, University Hospital Augsburg, Stenglinstrasse 2, 86156 Augsburg, Germany. E-mail: Monika.Jering@uk-augsburg.de

image, slow shear waves are displayed in blue and fast shear waves, corresponding to stiffer tissue, in red, on a scale of 0.5−10.0 m/s (Matsuzuka et al. 2015; Cheng et al. 2016; Zengel et al. 2018).

The advantage of VTIQ is that smaller regions of interest can be selected, and therefore, even small lesions can be characterized based on tissue stiffness, and multiple regions of interest can be evaluated simultaneously as illustrated in Figure 1 (Zengel et al. 2018). Although well validated for breast, thyroid and hepatic pathologies, tissue elastography has not been validated as a diagnostic tool in the evaluation of parotid gland lesions (Cantisani et al. 2014; Platz Batista da Silva et al. 2016; He et al. 2017). VTIQ combines qualitative and quantitative information and could therefore improve the differentiation between benign and malignant parotid lesions (Rubini et al. 2020).

Lesions in the parotid gland comprise 2%−6% of all head and neck tumors. While the majority are benign, approximately 20% are malignant (Mansour et al. 2017; Zengel et al. 2018). In the past 20 years surgery of benign parotid lesions has evolved in the direction of less invasive procedures, including extracapsular dissection and partial superficial parotidectomy (Mantsopoulos et al. 2015a, 2015b, 2015c, 2015d; Psychogios et al. 2020a). Although these surgical techniques have an excellent morbidity profile, particularly with regard to reducing the risk of facial nerve paralysis, in the case of an unexpected malignancy, a re-operation becomes necessary. As re-operations carry an increased risk of complications, improving pre-operative detection of malignant tumors becomes even more important. The aim of this study was to identify sonographic characteristics of benign and malignant parotid lesions with the use of high-resolution ultrasound in combination with VTIQ elastography.

METHODS

We conducted a prospective study assessing imaging characteristics of parotid gland tumors before surgical resection, using B-mode and color-coded Doppler ultrasound in addition to VTIQ. Patients referred for evaluation of a parotid gland lesion and undergoing a surgical procedure on the parotid gland at the University Hospital Augsburg between May 2017 and November 2019 were eligible for inclusion in this study. Metastases of cutaneous squamous cell carcinomas (SCCs) were also included if they were found within the parotid gland. The investigators performing the ultrasound and VTIQ were blinded to the patients' past medical and surgical history. Exclusion criteria included lack of prior surgical intervention or irradiation of the parotid region, a diagnosis of lymphoma, lack of the patient's ability to consent and missing sonographic data.

The local ethics committee approved the study protocol, and participants provided written, informed consent (2017/20).

A pre-operative, routine ultrasound was performed by three experienced clinical investigators on all study participants, using the Acuson S2000 (Probe 9 L4, Siemens Medical Solution, Erlangen, Germany) and a linear transducer (4.0−9.0 MHz). The size of the tumor in three dimensions and VTIQ measurements were recorded. Echogenicity of the tumor, lesion margins, vascularization pattern, vascularization location and presence of cystic structures on B-mode ultrasound were documented. Vascularization location was categorized as central, peripheral and avascular. At least three different quantitative VTIQ measurements were obtained, two within the lesion (in areas corresponding to the slowest and fastest shear waves, respectively) and one in the adjacent healthy tissue, peripheral to the tumor as a reference (Fig. 1). Based on the color-coded map generated by VTIQ, shear wave velocity was measured in regions of slowest (color-coded in blue) and fastest (color-coded in red) shear waves within the parotid lesion, taking care to exclude cystic areas. These measurements of slow and fast shear waves were each repeated three times. "Maximal shear wave velocity" was defined as the average of three measurements in areas of fast shear waves. Mean shear wave velocity was defined as the average of all six VTIQ measurements obtained within the parotid tumor. VTIQ was only measurable in the range of 0.5−10.0 m/s; velocities exceeding 10.0 m/s (denoted as "high velocity" on the equipment) were recorded as 10.0 m/s.

On the basis of prior studies in salivary gland tumors, areas of soft tissue (defined as a shear wave velocity of <3.5 m/s) and stiff tissue (shear wave velocity >6.0 m/s) were categorized as involving <30%, 30%−70% and >70% of the entire tumor (Zengel et al. 2018; Ruger et al. 2020).

The data extracted from the patients' medical record included patient age, sex, surgical date, type of surgical procedure, size of the tumor in the surgical specimen, histologic result, minimal, maximal and mean shear wave velocity, peripheral shear wave velocity (in the tissue adjacent to the tumor), tumor margins, echogenicity and presence of necrosis, cystic areas or a stiff core. Margin homogeneity was determined by B-mode ultrasound and defined as described by previous studies (Klintworth et al. 2012). A stiff core is a well-defined area within a lesion with a central zone of faster shear waves surrounded by tissue with slower shear waves and is characteristic of pleomorphic adenomas (PLA) (Klintworth et al. 2012). Necrosis was defined by B-mode ultrasound as ill-defined lesion margins with hypo-echoic areas and no perfusion.

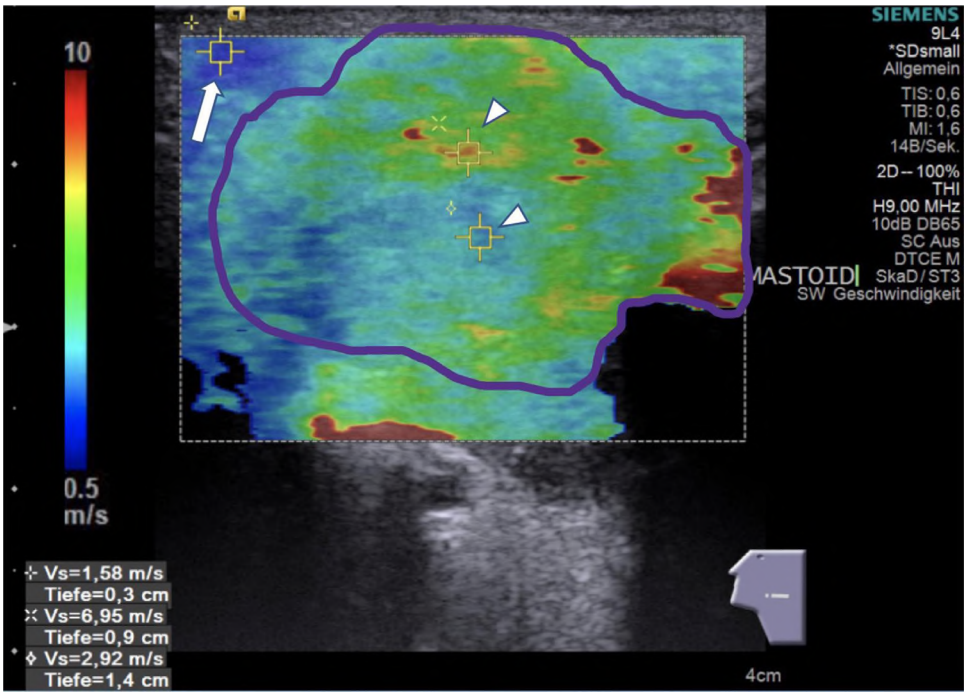

Fig. 1. Virtual Touch imaging quantification (VTIQ) of a pleomorphic adenoma. Pleomorphic adenoma on VTIQ image with shear wave velocities ranging from 1.58 to 6.95 m/s. Selected regions of interest, in which VTIQ measurements were performed, are represented by *yellow squares*. Two measurements were obtained within the lesion in areas of slowest (color-coded in *blue*) and fastest (color-coded in *red*) shear waves (*arrowheads*). Additionally, one measurement was performed in healthy tissue outside of the parotid lesion ("peripheral shear wave velocity") (*arrow*). The *purple line* delineates the margins of the pleomorphic adenoma.

When malignancy was suspected based on imaging findings, a core needle biopsy was performed for additional tissue characterization. Surgical procedures were adapted to results from the core needle biopsy and to the location of the parotid gland lesion: extracapsular dissection, partial parotidectomy, superficial parotidectomy or total parotidectomy. Postoperative histologic results were compared with tumor characteristics on the preoperative ultrasound examination. Three cases, in which both benign and malignant entities were identified on histology, were classified as malignant as the malignant phenotype predominated and accounted for most of the excised tissue (patient 1: Warthin tumor [WT] and Merkel cell carcinoma, patient 2: WT and metastasis of a SCC, patient 3: oncocytoma and Merkel cell carcinoma). Previous studies have provided evidence of simultaneously occurring lesions of different tumor dignity within the ipsilateral parotid gland (Curry et al. 2002; Heine et al. 2018).

Data are expressed as the mean (standard deviation) for continuous variables and the frequency (percentage) for categorical variables. Baseline characteristics of patients with benign and malignant tumors were compared with Student's *t*-test and Pearson's χ^2-test where appropriate. Univariate logistic regression models were used to examine the association between pre-operative ultrasound findings and tumor dignity obtained from histology. Models were furthermore adjusted for ill-defined tumor margins, presence of necrosis and vascularization pattern. The diagnostic accuracy of the following models in predicting malignant dignity was assessed using area under the receiver operating characteristic (ROC) curve (AUC) analyses and compared using the DeLong test: (i) ill-defined margins on B-mode ultrasound; (ii) mean shear wave velocity; (iii) stiff areas, defined as the proportion of the parotid tumor (categorized as $<30\%$, $30\%-70\%$ and $>70\%$) with a shear wave velocity >6.0 m/s; (iv) presence of necrosis and vascularization pattern; and (v) mean shear wave velocity necrosis and vascularization pattern. Statistical significance was assessed using a two-side α level of 0.05 without adjustment for multiplicity. All analyses were performed using STATA (Version 14.2, Stata Corp., College Station, TX, USA).

RESULTS

Of the 268 patients included in this study, 213 (79.4%) were diagnosed with a benign tumor and 55 (20.6%) with a malignant tumor based on histopathology. We were able to identify 13 different malignant

entities and 18 benign entities. The most commonly diagnosed benign lesion was a WT (n = 97, 45.5%), and the most commonly diagnosed malignancy was metastasis of a SCC (n = 29, 52.7%), which seems consistent with current literature (Franzen et al. 2019; Psychogios et al. 2020b). We compared all patients with malignancy (n = 55) to patients with benign tumors (n = 213).

Baseline characteristics of the 268 patients diagnosed with benign and malignant tumors of the parotid gland are summarized in Table 1. Patients with malignancy were older compared with those diagnosed with a benign lesion (75.5 ± 12.2 y vs. 58.3 ± 14.9 y, $p < 0.001$). Ill-defined tumor margins were more commonly visualized in malignant tumors (98.2%) than in benign lesions (4.2%, $p < 0.001$). Necrotic components were present in 45.5% of malignant and 0.9% of benign tumors ($p < 0.001$). Mean shear wave velocity was significantly higher in malignant than in benign tumors (6.3 ± 1.4 m/s vs. 4.7 ± 1.5 m/s, $p < 0.001$). Similarly, maximal shear wave velocity was significantly higher in malignant than in benign tumors (8.0 ± 1.8 m/s vs. 5.8 ± 2.0 m/s, $p < 0.001$) (Table 1). Figure 2 illustrates the distribution of mean shear wave velocities by tumor dignity in our patient cohort, and Figure 3, the distribution of maximal shear wave velocities. A greater area with shear wave velocity <3.5 m/s was more common in benign parotid lesions, and a greater area with shear wave velocity >6.0 m/s was more frequently observed in malignant tumors (both p values <0.001) (Table 1).

Table 1. Baseline characteristics with respect to tumor dignity

	Benign tumor (n = 213)	Malignant tumor (n = 55)	p Value
Age (y)	58.3 ± 14.9	75.5 ± 12.2	<0.001
Female sex	93 (43.7%)	18 (32.7%)	0.14
Mean velocity (m/s)	4.7 ± 1.5	6.3 ± 1.4	<0.001
Maximal velocity (m/s)	5.8 ± 2.0	8.0 ± 1.8	<0.001
Minimal velocity (m/s)	3.6 ± 1.2	4.6 ± 1.3	<0.001
Peripheral velocity (m/s)	2.6 ± 0.5	2.8 ± 0.9	0.026
Tumor margins (ill-defined)	9 (4.2%)	54 (98.2%)	<0.001
Margins			<0.001
Homogeneous	155 (72.8%)	1 (1.8%)	
Polycyclic	50 (23.5%)	1 (1.8%)	
Undefined	8 (3.8%)	53 (96.4%)	
Echogenicity			<0.001
Hypo-echoic	107 (50.2%)	1 (1.8%)	
Hyperechoic	2 (0.9%)	0 (0%)	
Heterogeneous	104 (48.8%)	54 (98.2%)	
Perfusion			0.19
No perfusion	106 (49.8%)	23 (41.8%)	
Low perfusion	77 (36.2%)	27 (49.1%)	
High perfusion	30 (14.1%)	5 (9.1%)	
Vascularization pattern			<0.001
Avascular	107 (50.5%)	23 (41.8%)	
Central	84 (39.6%)	12 (21.8%)	
Peripheral	21 (9.9%)	20 (36.4%)	
Area of low tissue stiffness (shear wave velocity <3.5 m/s)			<0.001
<30%	91 (42.7%)	49 (89.1%)	<0.001
30%–70%	47 (22.1%)	3 (5.5%)	<0.001
>70%	75 (35.2%)	3 (5.5%)	<0.001
Area of high tissue stiffness (shear wave velocity >6 m/s)			<0.001
<30%	171 (80.3%)	14 (25.5%)	<0.001
30%–70%	37 (17.4%)	31 (56.4%)	<0.001
>70%	5 (2.3%)	10 (18.2%)	<0.001
Stiff core*	54 (25.4%)	2 (3.6%)	<0.001
Structure			<0.001
Cystic	103 (48.6%)	0 (0%)	
Honeycomb	37 (17.5%)	0 (0%)	
Pigmented	37 (17.5%)	1 (1.8%)	
Undefined	35 (16.5%)	54 (98.2%)	
Areas of unmeasurable VTIQ†	69 (32.4%)	1 (1.8%)	<0.001
Distal enhancement	100 (46.9%)	1 (1.8%)	<0.001
Necrosis	2 (0.9%)	25 (45.5%)	<0.001

Values are reported as the frequency (%) or mean ± standard deviation.
VTIQ = Virtual Touch imaging quantification.
* A stiff core is defined as a central zone with a velocity >6.0 m/s with softer tissue in the vicinity.
† Lesions with cystic components in which VTIQ was not measurable. In all cases, VTIQ could be measured in non-cystic areas.

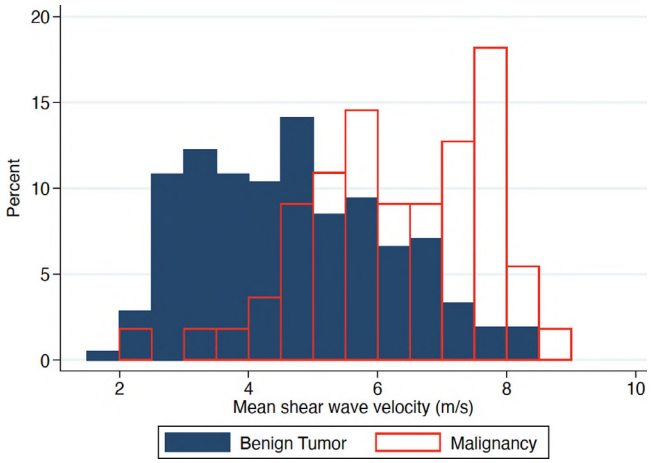

Fig. 2. Distribution of mean shear wave velocities (measured in m/s) within a parotid gland lesion with respect to tumor dignity. Mean shear wave velocity was calculated as the average of three distinct Virtual Touch imaging quantification (VTIQ) measurements in areas of slow shear waves and three distinct VTIQ measurements in areas of fast shear waves. Benign tumors are illustrated in *blue*, and malignant tumors in *red*.

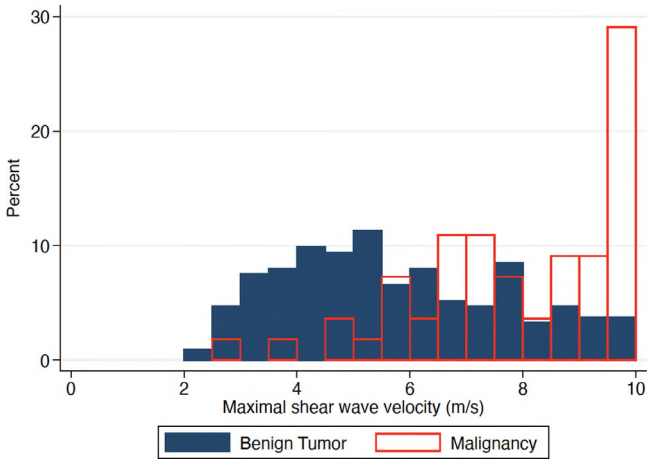

Fig. 3. Distribution of maximal shear wave velocities (measured in m/s) within a parotid gland lesion with respect to tumor dignity. ''Maximal'' shear wave velocity was defined as the mean of three distinct Virtual Touch imaging quantification measurements in areas of fast shear waves. Benign tumors are illustrated in *blue*, and malignant tumors in *red*.

Representative B-mode ultrasound and VTIQ images of a benign WT and a malignant tumor (SCC) are provided in Figures 4 and 5, respectively. The vascularization pattern of a PLA is illustrated in Figure 6.

Among the 213 benign lesions, WTs (n = 97, 45.5%) and PLAs (n = 67, 31.5%) were the most commonly identified entities. WTs contained a variable amount of cystic areas and, therefore, varied in stiffness. Because of the high fluid content of WTs, VTIQ could not be performed in cystic areas within the lesion in 54.0% of patients with WTs but was acquired in non-cystic areas within WTs in all cases, as illustrated in Figure 4. Cystic areas were detected in 86.5% of WTs versus 1.5% of PLAs ($p < 0.001$). Margins were homogeneous in 99.0% of WTs, and polycyclic in 68.7% and homogeneous in 29.9% of PLAs ($p < 0.001$). Tumor vascularization was central in 51.5% of patients with WTs and absent in most patients with PLAs (58.2%). In patients with WTs, almost half (n = 46, 47.4%) had predominantly tissue of low stiffness (>70% of the tumor with shear wave velocity <3.5 m/s), whereas in patients with PLAs, the majority (n = 46, 68.7%) had little tissue of low stiffness (<30% of the tumor). Most PLAs had a stiff core (n = 50, 74.6%) with high shear wave velocities (maximal velocity: 7.0 ± 1.9 m/s).

Among the 55 malignant tumors, the most common histologic diagnoses were SCC (n = 29, 46.8%) and acinus cell carcinoma (n = 3, 5.5%). All patients with SCC and acinus cell carcinoma had ill-defined tumor margins

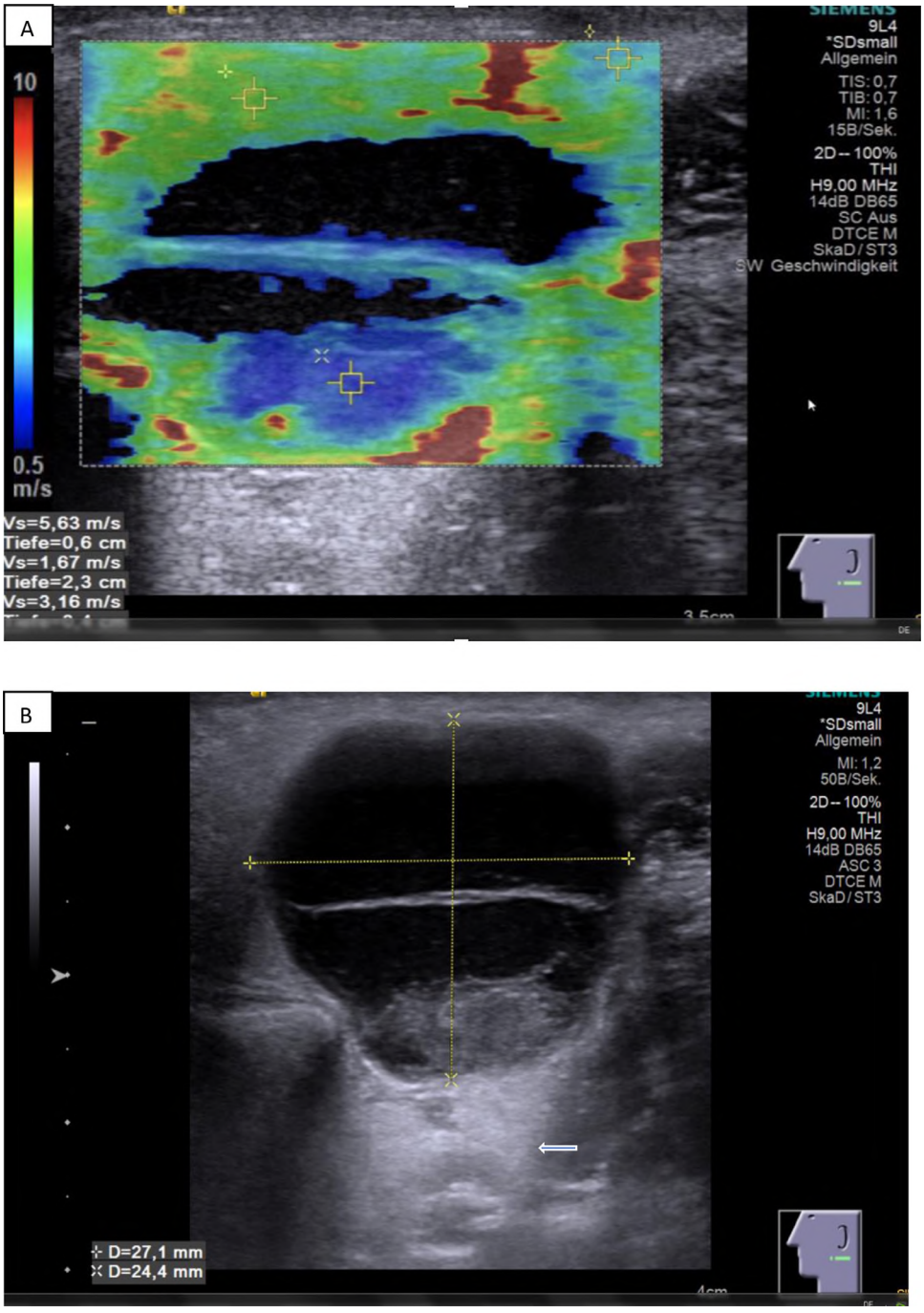

Fig. 4. Representative (a) Virtual Touch imaging quantification (VTIQ) and (B) B-mode ultrasound images of a Warthin tumor (WT). (a) Shear wave velocities on the color-coded map generated by VTIQ range from 3.16 to 5.63 m/s. Shear wave velocity cannot be measured in cystic areas by VTIQ, and therefore, cystic areas are not color-coded. Shear wave velocity measurements were obtained in surrounding tissue within the WT for analysis. Regions of interest where VTIQ measurements were performed are denoted by *small yellow squares*. (b) WT on B-mode ultrasound with distal enhancement (*arrow*).

on B-mode ultrasound, defined as indistinct and not circumscribed margins (Fig. 5). Although acinus cell carcinomas exhibited no perfusion, SCCs had a peripheral vascularization pattern in 40.7% of cases. Compared with acinus cell carcinoma, SCC had significantly higher mean (6.8 ± 1.1 m/s vs. 5.5 ± 1.1 m/s) and maximal shear wave (8.5 ± 1.4 m/s vs. 6.8 ± 2.1 m/s) velocities (all p values <0.001). In 96.3% of SCC cases, areas of

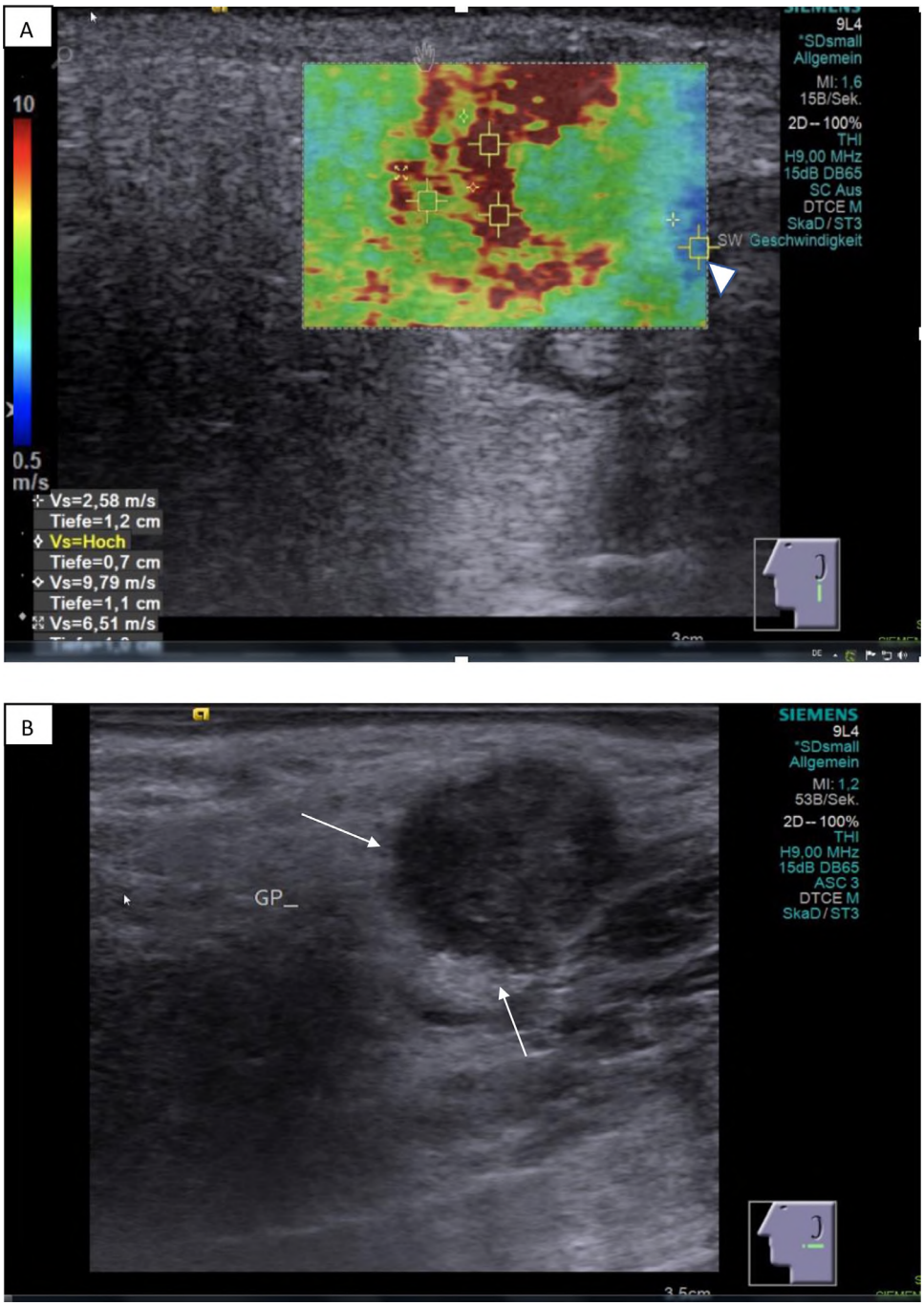

Fig. 5. Representative B-mode ultrasound and Virtual Touch imaging quantification (VTIQ) of a malignant tumor. (a) VTIQ image of a squamous cell carcinoma in the left parotid gland. VTIQ measurements were obtained within the lesion in areas of slowest shear waves (color-coded in *green* in the image) and fastest shear waves (color-coded in *red*), as well as peripherally to the lesion (*arrowhead*). If shear wave velocities exceeded 10.0 m/s (denoted as Vs = "hoch" or high velocity on the equipment), the shear wave velocity was recorded as 10.0 m/s, as VTIQ only allows measurements of shear waves in the range 0.5 to 10.0 m/s. (b) Corresponding heterogeneous echogenicity on B-mode ultrasound with ill-defined margins (*arrows*).

low tissue stiffness (shear wave velocity <3.5 m/s) on VTIQ encompassed <30% of the tumor.

On univariate logistic regression, faster mean shear waves were associated with a significantly higher risk of malignancy (odds ratio [OR]: 2.04, 95% confidence interval [CI]: 1.61−2.57, per 1.0 m/s increase), as were ill-defined tumor margins on B-mode ultrasound (OR: 1224.0, 95% CI: 151.8−9872.7) and presence of

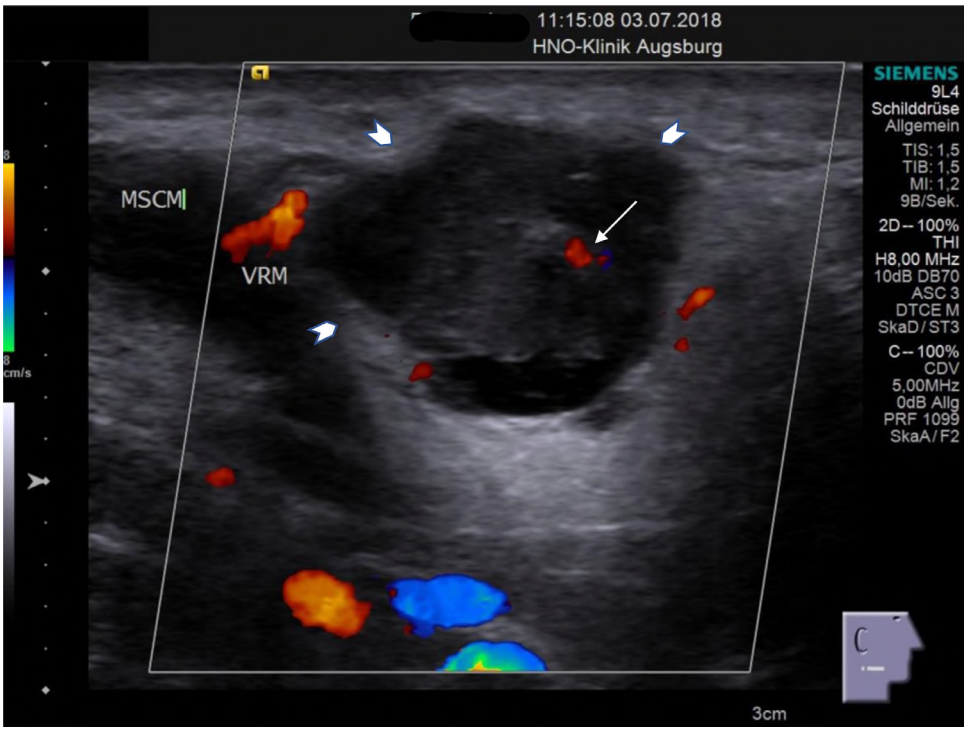

Fig. 6. Vascularization pattern on B-mode ultrasound in a pleomorphic adenoma. Central vascularization (*arrow*) of a pleomorphic adenoma with polycyclic lesion margins (*arrowhead*). MSCM = musculus sternocleidomastoideus; VRM = vena retromandibularis.

necrosis (OR: 87.9, 95% CI: 19.8–390.2). A graded relationship between the proportion of the tumor with high tissue stiffness (shear wave velocity >6.0 m/s) and the probability of malignancy was observed (OR: 10.23, 95% CI: 4.96–21.11 for 30%–70% of the tumor, and OR: 24.43, 95% CI: 7.33–81.42) for areas exceeding 70% with shear wave velocity >6.0 m/s. Risk relationships for mean shear wave velocity (OR: 1.87, 95% CI: 1.40–2.49) and stiff areas (area >70%; OR: 14.23, 95% CI: 2.91–69.57) were attenuated when controlling for the presence of necrosis, ill-defined margins and location of vascularization pattern.

The diagnostic performance of various imaging parameters with respect to prediction of tissue dignity, compared with the reference standard of histopathology from the surgical specimen, was assessed using AUCs. Diagnostic performance of imaging parameters derived from pre-operative B-mode ultrasound (ill-defined margins) was compared against the diagnostic performance of parameters derived from VTIQ (mean shear wave velocity and "stiff areas," defined as the proportion of the parotid tumor with shear waves >6.0 m/s using DeLong's method). AUC curve analyses revealed that ill-defined tumor margins on B-mode ultrasound had the highest diagnostic performance in predicting malignancy (AUC: 0.97, 95% CI: 0.95–0.99) compared with mean shear wave velocity on VTIQ alone (AUC: 0.78, 95% CI: 0.71–0.85) or the proportion of the tumor with high tissue stiffness (shear wave velocity >6.0 m/s) (AUC: 0.78, 95% CI: 0.72–0.85) ($p < 0.001$) (Fig. 7).

Diagnostic performance was improved when presence of necrosis and location of vascularization were added to mean shear wave velocity (AUC: 0.89, 95% CI: 0.83–0.94) and stiff areas (AUC: 0.90, 95% CI: 0.86–0.95), respectively (Fig. 8). Despite improved diagnostic accuracy with addition of necrosis and vascularization patterns to the VTIQ parameters of mean shear wave velocity and stiff areas, ill-defined tumor margin had the highest AUC (AUC: 0.97, 95% CI: 0.95–0.99) ($p < 0.001$) (Fig. 8).

Univariate logistic regression revealed a high predictive ability for a PLA when a stiff core was recognized (OR: 282.35, 95% CI: 36.51–2183.56) ($p < 0.001$).

DISCUSSION

The aim of this prospective study was to define sonographic imaging characteristics of benign and malignant parotid gland tumors and to investigate the diagnostic performance of multimodal ultrasonography using B-mode ultrasound in combination with VTIQ in differentiating benign from malignant parotid tumors. We found that ill-defined tumor margins on B-mode ultrasound were the strongest indicator of malignancy.

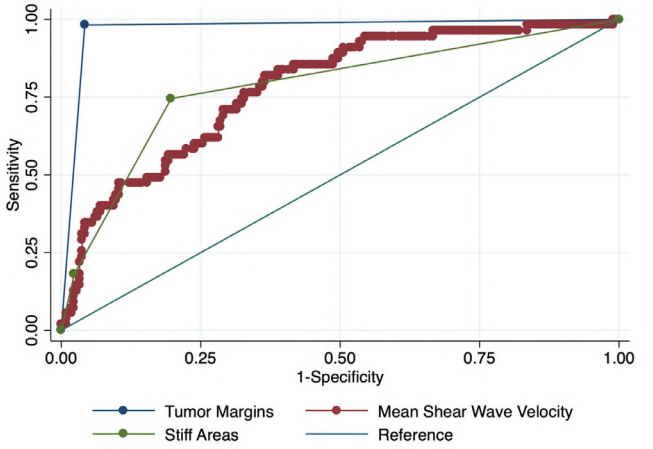

Fig. 7. Diagnostic performance of ill-defined margins, mean shear wave velocity and stiff areas. Receiver operating characteristic (ROC) curves for model 1, plotting sensitivity versus specificity. ROC curves describe the diagnostic performance of the following imaging parameters obtained on pre-operative B-mode ultrasound and Virtual Touch imaging quantification to identify malignancy, compared with the reference standard of histopathology from surgical specimen: (i) ill-defined tumor margins, (ii) mean shear wave velocity (m/s) of the parotid tumor and (iii) proportion of the parotid tumor (categorized as <30%, 30%−70% or >70%) with shear wave velocity >6.0 m/s (stiff areas). The diagnostic accuracy with respect to tumor dignity is compared among these three imaging parameters using the DeLong test. The area under the curve (AUC) for ill-defined margins was 0.97 (95% confidence interval [CI]: 0.95−0.99); for mean shear wave velocity, the AUC was 0.78 (95% CI: 0.71−0.85); and for stiff areas, the AUC was 0.78 (95% CI: 0.72−0.85) ($p < 0.001$).

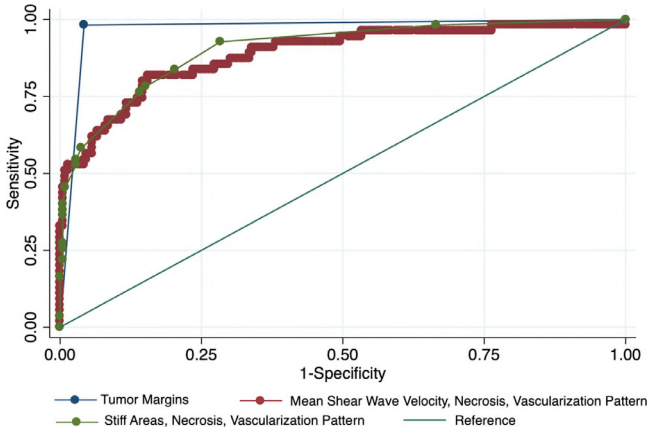

Fig. 8. Diagnostic performance of ill-defined margins, and models consisting of necrosis, vascularization pattern and mean shear wave velocity, or stiff areas. Receiver operating characteristic (ROC) curves for model 2, plotting sensitivity versus specificity. ROC curves describe the diagnostic performance of the following imaging parameters obtained on pre-operative B-mode ultrasound and Virtual Touch imaging quantification (VTIQ) to identify malignancy, compared with the references standard of histopathology from a surgical specimen: (i) ill-defined tumor margins; (ii) a combination of mean shear wave velocity, presence of necrosis and vascularization pattern; and (iii) a combination of stiff areas, presence of necrosis and vascularization pattern. The diagnostic accuracy with regards to tumor dignity is compared among these imaging parameters using DeLong test. The area under the curve (AUC) for ill-defined margins was 0.97 (95% confidence interval [CI]: 0.95−0.99); for a combination of mean shear wave velocity, necrosis and vascularization pattern, the AUC was 0.89 (95% CI: 0.83−0.94); and for a combination of stiff areas, necrosis and vascularization pattern, the AUC was 0.90 (95% CI: 0.86−0.95) ($p < 0.001$).

Nevertheless, inflamed benign tumors can also lead to poorly defined tumor margins (Mantsopoulos et al. 2015a, 2015b, 2015c, 2015d). Faster shear wave velocities and larger areas of stiff tissue were associated with increased risk for malignancy. Therefore, with additional non-invasive tissue characterization by VTIQ, more information on a parotid gland lesion is gained and diagnostic accuracy can be further improved.

Prior studies have indicated the importance of identifying malignant tumors in the parotid gland pre-operatively to optimize patient treatment and avoid repeat surgeries with their associated complications (Mantsopoulos et al. 2015b, 2015c). However, defining the tumor entity non-invasively before surgical intervention can be challenging because of the complexity and diversity of parotid lesions (Zengel et al. 2018). Ultrasound is a widely established imaging modality and constitutes an important, non-invasive tool in the evaluation of parotid lesions (Koischwitz et al. 2000; Heine et al. 2018). It is cheap, readily available and quick to perform although it is operator dependent. In contrast, measurement of tissue stiffness with VTIQ can provide a more objective assessment of tissue characteristics (Zengel et al. 2018). Although well validated in the evaluation of breast and thyroid malignancies, VTIQ to date has not been established as a tool in the evaluation of parotid masses (Athanasiou et al. 2010; Zhou et al. 2017).

Several previous studies evaluating VTIQ as a predictor for malignancy in the parotid gland have yielded conflicting results (Matsuzuka et al. 2015; Mansour et al. 2017; Zengel et al. 2018). Klintworth et al. (2012) reported a significant difference in characteristic patterns of tissue stiffness of parotid tumors. A subsequent meta-analysis derived from 10 studies (n = 711 patients) investigated the predictive ability of sonoelastography in distinguishing benign from malignant parotid lesions and reported limited discriminative ability with the use of VTIQ for malignant parotid tumors (Zhang et al. 2019). However, most of these studies included only a small number of patients with malignancy, limiting power. In contrast, in the present study, with a substantially larger cohort size and 55 patients diagnosed with malignancy, mean and maximal shear wave velocities were significantly higher in malignant compared with benign parotid tumors, though absolute differences in velocity were rather small. Nevertheless, faster shear waves were associated with a significantly higher risk of malignancy though risk relationships were attenuated on multivariate adjustment.

Concordant with results from Zhang et al.'s meta-analysis, malignant parotid tumors in the present study had stiffer tissue than benign lesions and therefore faster mean shear wave velocities on VTIQ. However, there was a considerable overlap in shear wave velocities among malignant and benign tumors in the present study. We hypothesize that this overlap may be related to the great variation in histologic dignity in the parotid gland. Some lesions, such as a WT, have a greater area of cystic elements. Within the cystic areas, VTIQ cannot be measured and therefore provides no additional information regarding tumor dignity in comparison to B-mode ultrasound. However, some WTs also present with soft areas, where VTIQ can be easily applied. Our study results indicated that WTs had slower shear wave velocities than PLAs. On the other hand, PLAs more frequently had a stiff core with faster shear wave velocities, making it difficult to distinguish PLAs from malignant tumors based on a single measurement of maximal shear wave velocity (Klintworth et al. 2012). Nevertheless, malignancies encompassed a greater area of fast shear wave velocities over 6.0 m/s in comparison to PLAs and other benign lesions. Therefore, a high proportion of the tumor with shear wave velocities >6.0 m/s is a strong indicator for malignancy.

In a study evaluating salivary gland lesions in patients with Sjogren's syndrome, Knopf et al. (2015) reported that mean shear wave elastography was able to perform well in the evaluation of salivary gland tumors. This study found slower mean shear wave velocities in healthy glandular tissue. The mean shear wave velocity measured in the healthy parotid tissue was 2.86 m/s, similar to the velocities measured in this study.

Matsuzuka et al. (2015) measured mean shear wave velocities on VTIQ of 4.24 ± 1.75 m/s in benign lesions. This study found that VTIQ had high discriminative power in differentiating between malignant and benign tumors, with an AUC of 97.1% (Matsuzuka et al. 2015). Our study was able to include a large patient cohort of malignant salivary gland lesions with a diverse representation of tumor entities. While mean shear wave velocity was associated with malignancy, these risk relationships were attenuated on multivariate adjustment. Although ill-defined margins on B-mode ultrasound had greater diagnostic performance, mean shear velocity nevertheless was found to have good discriminative accuracy in the differentiation of malignant from benign lesions. On the basis of shear wave velocity derived from VTIQ, pre-operative planning can be adapted, such as performing a core needle biopsy for dignity determination (Zbaren et al. 2018).

The strengths of this study include the prospective study design and the large number of parotid tumors with histologic verification from a surgical specimen rather than fine-needle aspirates and the diversity in pathologies (Mezei et al. 2018).

Our study should be interpreted in the context of its limitations. Ultrasonography was performed by trained and experienced investigators, and the diagnostic performance of B-mode ultrasound findings in relation to VTIQ may be less predictive in the hands of an inexperienced sonographer. The predictive ability of B-mode ultrasound in conjunction with VTIQ for a malignant lesion should be prospectively evaluated in a larger patient cohort by an inexperienced sonographer in a separate study. Lymphomas were excluded from the analysis because of the small sample size (n = 7) and because their imaging characteristics have been found to differ

from those of malignant tumors with slower shear waves on VTIQ compared with other malignancies (Okasha et al. 2014; Chae et al. 2019).

Furthermore, because of the small number of patients with lymphoma, our study was underpowered to assess differences in imaging characteristics between patients with lymphomas and those with other malignancies. Nevertheless, lymphomas can usually be diagnosed according to clinical signs on presentation and have a distinctive appearance on B-mode ultrasound similar to a "string of beads" (Bialek and Jakubowski 2017).

CONCLUSIONS

In our study, higher mean and maximal shear wave velocity on VTIQ and greater proportion of the tumor of high stiffness were associated with increased risk for malignancy in parotid gland tumors. Although the diagnostic performance of ill-defined tumor margins outperformed mean shear wave velocity and areas of high tissue stiffness, VTIQ by itself is predictive of malignancy. Benign tumors have slower shear wave velocity and less variation in velocities. By combining B-mode ultrasound with VTIQ, additional information on the dignity of a parotid mass may be gained, which can help optimize pre-operative planning and patient care.

Acknowledgments—This study was funded by Deutsche Gesellschaft für Ultraschall in der Medizin (DEGUM) through Grant No. DEGUM_2018.07.03.

Conflict of interest disclosure—The authors have no conflicts of interest to declare.

REFERENCES

Athanasiou A, Tardivon A, Tanter M, Sigal-Zafrani B, Bercoff J, Deffieux T, Gennison JL, Neuenschwander S. Breast lesions: Quantitative elastography with supersonic shear imaging—Preliminary results. Radiology 2010;256:297–303.

Azizi G, Keller JM, Mayo ML, Piper K, Puett D, Earp KM, Malchoff CD. Shear wave elastography and cervical lymph nodes: Predicting malignancy. Ultrasound Med Biol 2016;42:1273–1281.

Bialek EJ, Jakubowski W. Mistakes in ultrasound diagnosis of superficial lymph nodes. J Ultrason 2017;17:59–65.

Bozzato A. Interpretation of ultrasound findings in otorhinolaryngology: Salivary glands, paraganglioma, angioma, esophagus, hypopharynx, extra cranial vessels and temporomandibular joint. HNO 2015;63:453–465 quiz 466−457.

Cantisani V, Lodise P, Grazhdani H, Mancuso E, Maggini E, Di Rocco G, D'Ambrosio F, Calliada F, Redler A, Ricci P, Catalano C. Ultrasound elastography in the evaluation of thyroid pathology: Current status. Eur J Radiol 2014;83:420–428.

Chae SY, Jung HN, Ryoo I, Suh S. Differentiating cervical metastatic lymphadenopathy and lymphoma by shear wave elastography. Sci Rep 2019;9:12396.

Cheng KL, Choi YJ, Shim WH, Lee JH, Baek JH. Virtual Touch tissue imaging quantification shear wave elastography: Prospective assessment of cervical lymph nodes. Ultrasound Med Biol 2016;42:378–386.

Curry JL, Petruzzelli GJ, McClatchey KD, Lingen MW. Synchronous benign and malignant salivary gland tumors in ipsilateral glands: A report of two cases and a review of literature. Head Neck 2002;24:301–306.

Franzen A, Lieder A, Guenzel T, Buchali A. The Heterogenicity of Parotid Gland Squamous Cell Carcinoma: A Study of 49 Patients. In Vivo 2019;33(6):2001–2006.

He YP, Xu HX, Li XL, Li DD, Bo XW, Zhao CK, Liu BJ, Wang D, Xu HX. Comparison of Virtual Touch Tissue imaging & quantification (VTIQ) and Toshiba shear wave elastography (T-SWE) in diagnosis of thyroid nodules: Initial experience. Clin Hemorheol Microcirc 2017;66:15–26.

Heine D, Zenk J, Psychogios G. Two case reports of synchronous unilateral pleomorphic adenoma and cystadenolymphoma of the parotid gland with literature review. J Ultrason 2018;18:369–373.

Klintworth N, Mantsopoulos K, Zenk J, Psychogios G, Iro H, Bozzato A. Sonoelastography of parotid gland tumours: Initial experience and identification of characteristic patterns. Eur Radiol 2012;22:947–956.

Knopf A, Hofauer B, Thurmel K, Meier R, Stock K, Bas M, Manour N. Diagnostic utility of acoustic radiation force impulse (ARFI) imaging in primary Sjoegren's syndrome. Eur Radiol 2015;25:3027–3034.

Koischwitz D, Gritzmann N. Ultrasound of the neck. Radiol Clin North Am 2000;38:1029–1045.

Mansour N, Bas M, Stock KF, Strassen U, Hofauer B, Knopf A. Multimodal ultrasonographic pathway of parotid gland lesions. Ultraschall Med 2017;38:166–173.

Mantsopoulos K, Klintworth N, Iro H, Bozzato A. Applicability of shear wave elastography of the major salivary glands: Values in healthy patients and effects of gender, smoking and pre-compression. Ultrasound Med Biol 2015a;41:2310–2318.

Mantsopoulos K, Koch M, Klintworth N, Zenk J, Iro H. Evolution and changing trends in surgery for benign parotid tumors. Laryngoscope 2015b;125:122–127.

Mantsopoulos K, Psychogios G, Agaimy A, Kunzel J, Zenk J, Iro H, Bohr C. Inflamed benign tumors of the parotid gland: Diagnostic pitfalls from a potentially misleading entity. Head Neck 2015c;37:23–29.

Mantsopoulos K, Velegrakis S, Iro H. Unexpected detection of parotid gland malignancy during primary extracapsular dissection. Otolaryngol Head Neck Surg 2015d;152:1042–1047.

Matsuzuka T, Suzuki M, Saijo S, Ikeda M, Matsui T, Nomoto Y, Nomoto M, Imaizumi M, Tada Y, Omori K. Stiffness of salivary gland and tumor measured by new ultrasonic techniques: Virtual Touch quantification and IQ. Auris Nasus Larynx 2015;42:128–133.

Mezei T, Mocan S, Ormenisan A, Baroti B, Iacob A. The value of fine needle aspiration cytology in the clinical management of rare salivary gland tumors. J Appl Oral Sci 2018;26 e20170267.

Okasha HH, Mansour M, Attia KA, Khattab HM, Sakr AY, Naguib M, Aref W, Al-Naggar AA, Ezzat R. Role of high resolution ultrasound/endosonography and elastography in predicting lymph node malignancy. Endosc Ultrasound 2014;3:58–62.

Platz Batista da Silva N, Schauer M, Hornung M, Lang S, Beyer LP, Wiesinger I, Stroszczynski C, Jung EM. Intrasurgical dignity assessment of hepatic tumors using semi-quantitative strain elastography and contrast-enhanced ultrasound for optimisation of liver tumor surgery. Clin Hemorheol Microcirc 2016;64:735–745.

Psychogios G, Rueger H, Jering M, Tsoures E, Kunzel J, Zenk J. Ultrasound can help to indirectly predict contact of parotid tumors to the facial nerve, correct intraglandular localization, and appropriate surgical technique. Head Neck 2019;41:3211–3218.

Psychogios G, Bohr C, Constantinidis J, Canis M, Vander Poorten V, Plzak J, Knopf A, Betz C, Gutinas-Lichius O, Zenk J. Review of surgical techniques and guide for decision making in the treatment of benign parotid tumors. Eur Arch Otorhinolaryngol 2020a;277:2081–2084.

Psychogios G, Vlastos I, Thölken R, Zenk J. Warthin's tumour seems to be the most common benign neoplasm of the parotid gland in Germany. Eur Arch Otorhinolaryngol 2020b;277:2081–2084.

Rubini A, Guiban O, Cantisani V, D'Ambrosio F. Multiparametric ultrasound evaluation of parotid gland tumors: B-Mode and color Doppler in comparison and in combination with contrast-enhanced ultrasound and elastography: A case report of a misleading diagnosis. J Ultrasound 2020. doi: 10.1007/s40477-020-00469-4. Accessed May 6th 2020. [e-pub ahead of print].

Ruger H, Psychogios G, Jering M, Zenk J. Multimodal ultrasound including Virtual Touch imaging quantification for

differentiating cervical lymph nodes. Ultrasound Med Biol 2020;46:2677–2682.
Zbaren P, Triantafyllou A, Devaney KO, Poorten VV, Hellquist H, Rinaldo A, Ferlito A. Preoperative diagnostic of parotid gland neoplasms: Fine-needle aspiration cytology or core needle biopsy? Eur Arch Otorhinolaryngol 2018;275:2609–2613.
Zengel P, Notter F, Clevert DA. VTIQ and VTQ in combination with B-mode and color Doppler ultrasound improve classification of salivary gland tumors, especially for inexperienced physicians. Clin Hemorheol Microcirc 2018;70:457–466.
Zhang YF, Li H, Wang XM, Cai YF. Sonoelastography for differential diagnosis between malignant and benign parotid lesions: A meta-analysis. Eur Radiol 2019;29:725–735.
Zhou H, Zhou XL, Xu HX, Li DD, Liu BJ, Zhang YF, Xu JM, Bo XW, Li XL, Guo LH, Qu S. Virtual Touch tissue imaging and quantification in the evaluation of thyroid nodules. J Ultrasound Med 2017;36:251–260.